ELSEVIER

Materials Science and Engineering A292 (2000) 90–95

MATERIALS SCIENCE & ENGINEERING A

www.elsevier.com/locate/msea

Erosion- and wear-corrosion behavior of Fe–Mn–Al alloys in NaCl solution

Her-Hsiung Huang [a,*], Tung-Han Chuang [b]

[a] *Institute of Dental Materials, School of Dentistry, Chung-Shan Medical and Dental College, Taichung, Taiwan, ROC*
[b] *Institute of Materials Science and Engineering, National Taiwan University, Taipei, Taiwan, ROC*

Received 30 December 1999; received in revised form 17 April 2000

Abstract

The erosion- and wear-corrosion behavior of solution-annealed and age-treated Fe–Mn–Al alloys in aerated 3% NaCl solution were investigated using a self-made rotating cylinder electrode system. The results showed that the open circuit potentials of Fe–Mn–Al alloys in 3% NaCl solution increased with increasing rotation speed during the erosion-corrosion test, but decreased with increasing rotation speed and contact load during the wear-corrosion test. Potentiodynamic polarization curves showed that the Fe–Mn–Al alloys had no passive region during erosion- and wear-corrosion tests, except that the solution-annealed specimen had an active-to-passive transition behavior during the erosion-corrosion test. After potentiodynamic polarization curve measurements during erosion- and wear-corrosion tests, the ferrite phase in solution-annealed Fe–Mn–Al alloy was prone to corrode with respect to the austenite phase. However, for age-treated Fe–Mn–Al alloy, corrosion preferentially occurred in the austenite phase region where β-Mn precipitated.

Keywords: Erosion-corrosion; Wear-corrosion; Fe–Mn–Al alloy; NaCl; Aging treatment

1. Introduction

Conventional Fe–Cr–Ni alloys have been widely used in industries owing to their adequate corrosion resistances and mechanical properties. However, on the basis of economic and strategic considerations, Fe–Mn–Al alloys could be good candidates for replacing at least some conventional Fe–Cr–Ni stainless steels [1–3]. Studies concerning the corrosion behavior of Fe–Mn–Al alloys in chloride solution have been reported extensively [4–10]. Wang and Rapp [4] found that the ferritic Fe–Mn–Al alloys, with respective Al and Mn contents less than 10 and 8 wt.%, have better electrochemical properties than Fe–10Cr alloy in artificial seawater. Wang and Beck [5] reported that cast Fe–30Mn–10Al–C–Si alloy has a lower corrosion rate than 18Cr–9Ni–Ti stainless steel in artificial seawater. On the other hand, Tsai et al. [9] reported that the corrosion resistances of austenitic Fe–Mn–Al alloys in chloride solutions are inferior to that of AISI 316 stainless steel. However, only limited information concerning the erosion- or wear-corrosion (a complex phenomenon involving the interactions of mechanical, metallurgical and chemical factors) of Fe–Mn–Al alloy is available in the literature [5,10]. Furthermore, the relative corrosion resistance between the ferrite and austenite phases for a duplex Fe–Mn–Al alloy is interesting and worth further investigation.

In this investigation, the erosion- and wear-corrosion behavior of Fe–Mn–Al alloy, with a ferrite/austenite structure, in aerated 3% NaCl solution were investigated using a self-made rotating cylinder electrode system. The effect of precipitation phase on the erosion- and wear-corrosion behavior of Fe–Mn–Al alloy after age heat treatment was also proposed.

2. Experimental procedure

The chemical composition (in wt.%) of the Fe–Mn–Al alloy used was 32.1Mn–12.7Al–3.05Cr–0.86C, and Fe as balance. The Fe–Mn–Al alloy was solution-an-

* Corresponding author. Tel.: +886-4-4718668; fax: +886-4-4759065.
E-mail address: hhhuang@mercury.csmc.edu.tw (H.-H. Huang).

0921-5093/00/$ - see front matter
PII: S0921-5093(00)01021-2

nealed treated at 1050°C for 1 h and then oil quenched. Aging heat treatment at 800°C for 10 h was made for the solution-annealed specimen. The solution-annealed and age-treated Fe–Mn–Al alloys were designated as specimens SA and AT, respectively. The hardnesses of specimens SA and AT were HR_B 64 and HR_B 75, respectively.

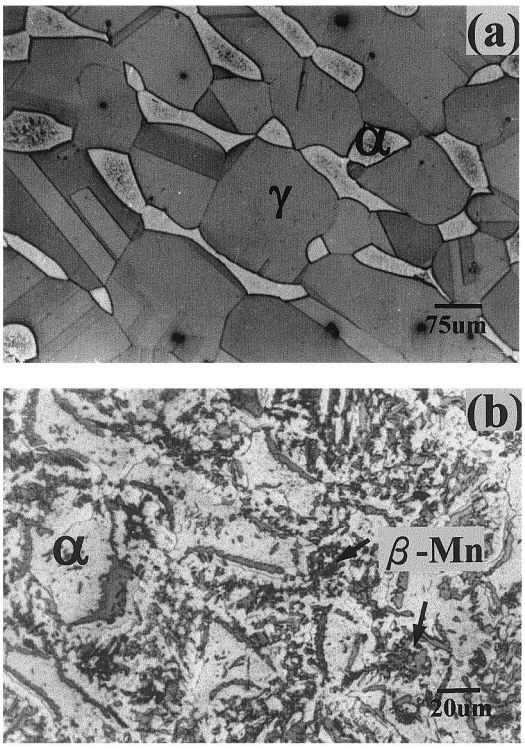

Fig. 1. Optical micrographs of (a) solution-annealed (specimen SA) and (b) age-treated (specimen AT) Fe–Mn–Al alloys.

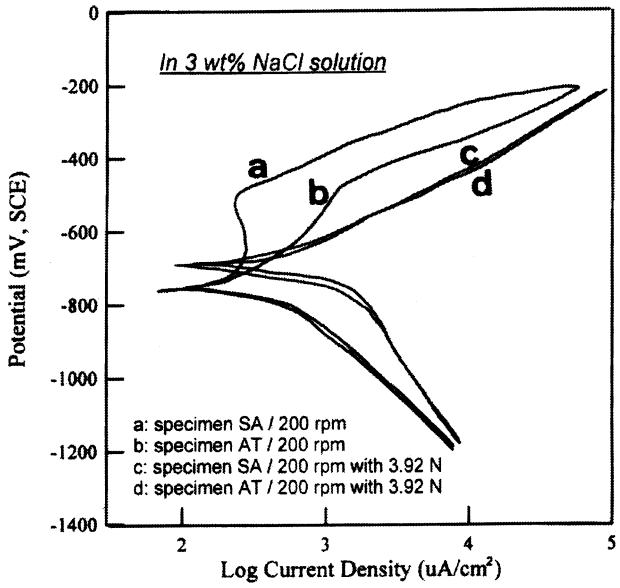

Fig. 2. Potentiodynamic polarization curves of specimens SA and AT in 3% NaCl solution (curves a and b: under loading free conditions (0 N/200 rev. min^{-1}); curves c and d: under loading conditions (3.92 N/200 rev. min^{-1})).

A self-made rotating cylinder electrode system (block-on-cylinder) was used for erosion- and wear-corrosion tests. The dimension of the cylindrically-shaped metal specimen was 15 mm long and 20 mm in diameter. The specimen was inlaid to a rotating rod driven by a motor. An alumina block was used to apply a load on the specimen during the wear-corrosion test. The contact width between the cylindrical metal specimen and the alumina block was 5 mm. The Fe–Mn–Al specimen and alumina block were ground with SiC paper to 1000 grit before the corrosion test. The erosion- and wear-corrosion tests were conducted in an aerated 3% NaCl solution (pH 6). The open-circuit potential (OCP) and potentiodynamic polarization curve (from -1200 to -200 mV_{SCE} with a scan rate of 1 mV s^{-1}) were measured using an EG & G Model 273 potentiostat. A saturated calomel electrode (SCE) was used as the reference electrode and platinum was used as the counter electrode. The contact load was the normal force applied on the specimen through the alumina block. The rotation speed was varied from 0 to 1000 rev. min^{-1}, while the contact load was in the range from 0.49 to 11.76 N. The weight losses of the specimens after wear-corrosion tests were measured by weighing the specimens periodically up to 90 h.

The structure of the specimen tested was identified by X-ray diffraction (XRD). Chemical analysis of the precipitation phase after aging heat treatment was conducted with a wavelength dispersive spectrometer (WDS). After erosion- and wear-corrosion tests, the surfaces of the specimens were examined by scanning electron microscope (SEM).

3. Results and discussion

The optical micrographs of solution-annealed (specimen SA) and age-treated (specimen AT) Fe–Mn–Al alloys are shown in Figs. 1(a) and (b), respectively. The microstructure of specimen SA consisted of ferrite (α) and austenite (γ) phases (Fig. 1(a)). For specimen AT, β-Mn phase, which was identified by XRD and WDS, preferentially precipitated within the austenite grain (Fig. 1(b)). Information concerning the kinetics of the precipitation of β-Mn in Fe–Mn–Al alloy was reported elsewhere [11].

The potentiodynamic polarization curves of specimens SA and AT in 3% NaCl solution under loading free (200 rev. min^{-1}) and loading (3.92 N/200 rev. min^{-1}) conditions are shown in Fig. 2. As can be seen in this figure, under loading free conditions (erosion-corrosion process), the corrosion potentials (E_{corr}) of specimens SA and AT were around -760 mV_{SCE}. Furthermore, specimen SA exhibited an active-to-pas-

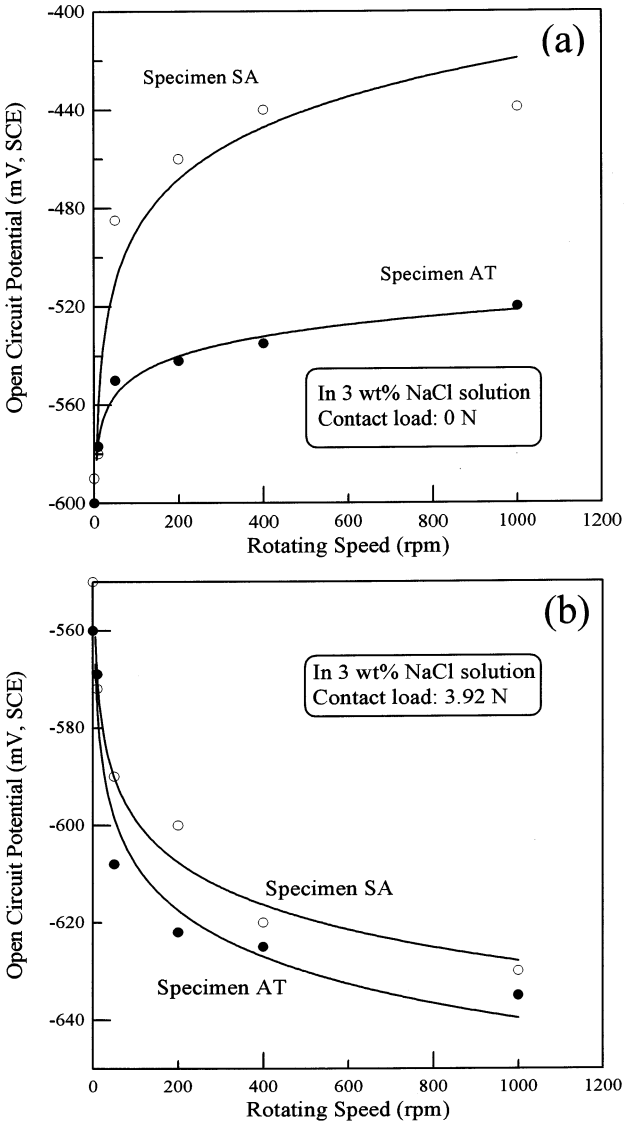

Fig. 3. Effect of rotation speed on the open circuit potential of specimens SA and AT in 3% NaCl solution under loading free and loading (3.92 N) conditions.

sive transition behavior (curve a), while no passive region could be found for specimen AT (curve b). However, under loading conditions (wear-corrosion process), specimens SA and AT (curves c and d) had similar anodic behavior, and the corresponding anodic current densities were much higher than those obtained under loading free conditions (curves a and b). Tsai et al. [9] have reported that either solution-annealed or age-treated austenitic Fe–Mn–Al alloy exhibits an active-to-passive transition behavior in 3.5% NaCl solution under loading free conditions. In the present investigation, by comparing curves a and b shown in Fig. 2, it was clear that the presence of β-Mn in specimen AT led to the disappearance of the passive region in the polarization curve under free loading conditions. Therefore, specimen AT (curve b) showed a higher anodic current density (about few times in magnitude) than specimen SA (curve a) under loading free conditions. On the other hand, under loading conditions, the contact load applied on the metal specimen could cause damage to the metal surface, resulting in much higher anodic current density (about few times to more than one order of magnitude) for specimens SA and AT (curves c and d) with respective to loading free conditions (curves a and b). Consequently, the disappearance of the passive region in the polarization curve of specimen SA under loading conditions (curve c in Fig. 2) was believed to be associated with the breakdown of the passive film on the metal surface by the abrasive process.

It was noted that the anodic slopes of curves c and d are different from those of curves a and b in Fig. 2. In addition, two anodic slopes for curves a and b indicated different dissolution mechanisms, which, however, needs further investigation. Furthermore, the anodic currents of curves c and d were very similar. In other words, specimens SA and AT had similar anodic behavior under loading conditions.

The effect of rotating speed on the OCPs of specimens SA and AT in 3% NaCl solution under loading free and loading (3.92 N) conditions is shown in Fig. 3. Under loading free conditions (Fig. 3(a)), the OCPs of specimens SA and AT increased with increasing rotation speed. However, under loading conditions (Fig. 3(b)), the difference in OCP between specimens SA and AT was small (around 5–22 mV). In addition, the OCPs of specimens SA and AT decreased with increasing rotating speed under loading conditions. During the erosion-corrosion test (Fig. 3(a)), the increase in OCP with rotation speed was associated with the accelerated transfer of dissolved oxygen to the metal surface by increasing the rotation speed. The SEM observation of the specimens after erosion-corrosion tests also revealed no significant corrosion attack on the metal surface. During wear-corrosion test (Fig. 3(b)), on the other hand, the decrease in OCP with increasing rotation speed was mainly due to the higher exposure area of fresh metal surface by increasing the rotation speed. In addition, the small difference in OCP between specimens SA and AT implied that the metallurgical effect on the difference in OCP between specimens SA and AT under loading conditions was not significant.

The effect of contact load on the OCPs of specimens SA and AT in 3% NaCl solution under constant rotating speed (200 rev. min^{-1}) is shown in Fig. 4. As shown in this figure, the OCPs of specimens SA and AT were nearly the same, and decreased gradually to about $-620\ mV_{SCE}$ when the contact load was over 7.84 N. This indicated that the contact load applied on the specimen would cause damage to the metal surface, resulting in the exposure of fresh metal. The area of the fresh metal surface would increase when the contact

load increased, leading to a more negative OCP. When the contact load was above 7.84 N, the area of fresh metal surface might reach a stable value. Consequently, the OCPs were nearly independent of the contact load applied.

The weight losses of specimens SA and AT during the wear tests in air and in 3% NaCl solution under 11.76 N and 200 rev. min^{-1} condition for various durations up to 90 h are shown in Fig. 5. It revealed that the weight losses of specimens SA and AT increased with an increase in wear duration. The weight losses after the wear test in air were more than eight times larger than those obtained in 3% NaCl solution. Furthermore, the weight loss of specimen SA during the 90-h wear test in 3% NaCl solution was about twice as large as that of specimen AT. The results shown in Fig. 5 indicated that the metal removal rate of Fe–Mn–Al alloy in air could be considered as the pure mechanical wear rate. The presence of NaCl solution could provide a good lubrication effect between the alumina block and the metal specimen, leading to a much lower weight loss during the wear test in NaCl solution as compared with that obtained in air. On the other hand, the presence of β-Mn phase in the age-treated specimen AT resulted in a higher hardness as compared with that of the solution-annealed specimen SA (specimen SA: HR_B 64; specimen AT: HR_B 75). Consequently, the fact that specimen AT had a lower weight loss than specimen SA during the wear test in either air or NaCl solution could be partly explained though the presence of brittle β-Mn phase reduces the ductility of the Fe–Mn–Al alloy [12].

As can be seen in Fig. 5, the weight losses of all specimens during the wear tests in either air or NaCl solution were in linear proportion to the test time, namely the sliding distance. Similar results have been reported by Nathan and Jones [13], the weight loss of metal by wear is proportional to the sliding distance.

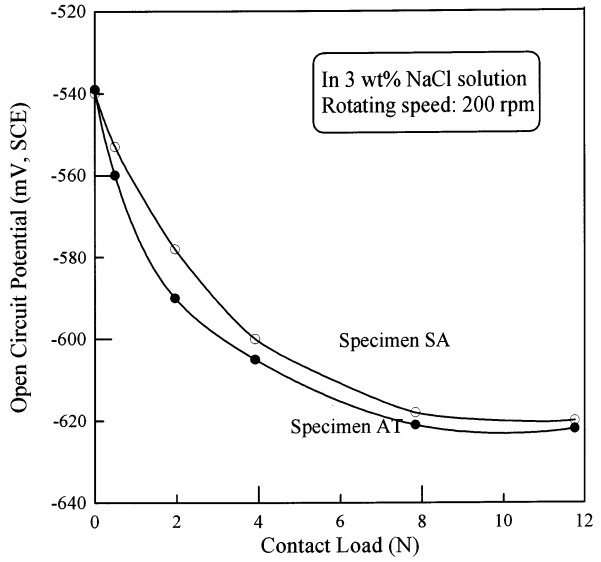

Fig. 4. Effect of contact load on the open circuit potential of specimens SA and AT in 3% NaCl solution under constant rotation speed (200 rev. min^{-1}).

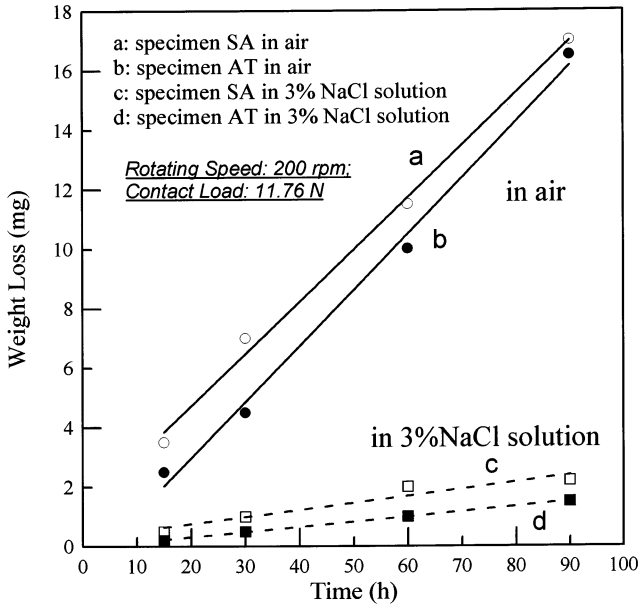

Fig. 5. Weight losses of specimens SA and AT during the wear tests in air and in 3% NaCl solution under 11.76 N and 200 rev. min^{-1} conditions for various durations up to 90 h.

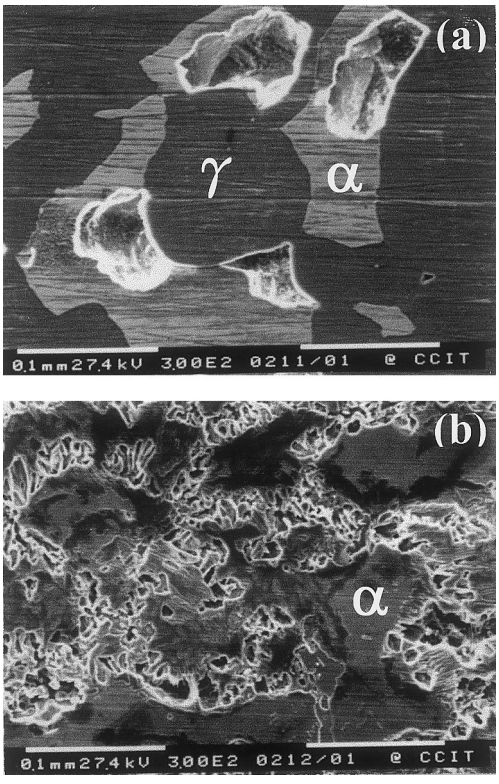

Fig. 6. SEM observations of specimens SA and AT after potentiodynamic polarization curve measurements in 3% NaCl solution under loading free conditions (200 rev. min^{-1}).

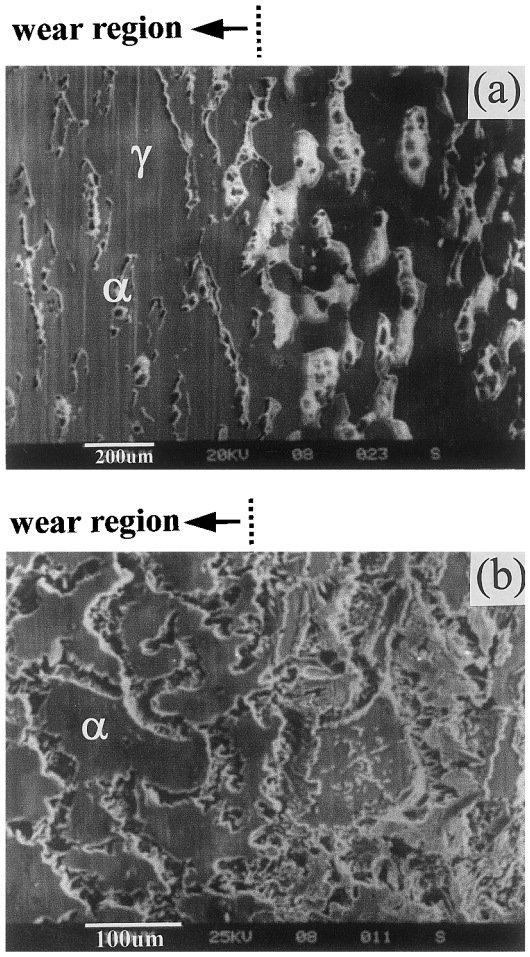

Fig. 7. SEM observations of specimens SA and AT after potentiodynamic polarization curve measurements in 3% NaCl solution under loading conditions (11.76 N/200 rev. min^{-1}).

The SEM observations of specimens SA and AT after potentiodynamic polarization curve measurements in 3% NaCl solution under loading free (200 rev. min^{-1}) and loading (11.76 N/200 rev. min^{-1}) conditions are shown in Figs. 6 and 7, respectively. After potentiodynamic polarization curve measurements, regardless of loading condition, pits were only observed at the ferrite (α) phase for specimen SA (Figs. 6(a) and 7(a)); for specimen AT, severe localized corrosion preferentially occurred at the austenite (γ) phase region where β-Mn precipitated, while the ferrite phase revealed good corrosion resistance (Figs. 6(b) and 7(b)). Chang et al. [12] have also reported that the pitting corrosion resistance of the ferrite phase is inferior to the austenite phase for a duplex (ferrite/austenite structure) Fe–Mn–Al alloy in 3.5% NaCl solution. In the present investigation, the austenite phase showed better corrosion resistance than the ferrite phase for solution-annealed Fe–Mn–Al alloy during erosion- and wear-corrosion tests in 3% NaCl solution. However, when β-Mn precipitated within the austenite grain in Fe–Mn–Al alloy after age heat treatment, the ferrite phase showed good localized corrosion resistance, and the austenite phase region corroded severely. Though the presence of hard β-Mn within the austenite phase provided a lower weight loss of Fe–Mn–Al alloy during wear-corrosion test (line d in Fig. 5), it significantly reduced the localized corrosion resistance of austenite phase in Fe–Mn–Al alloy in NaCl solution.

4. Conclusions

The potentiodynamic polarization curve of the solution-annealed Fe–Mn–Al alloy exhibited an active-to-passive transition behavior in 3% NaCl solution during the erosion-corrosion process, while no passive region could be found for the age-treated Fe–Mn–Al alloy. During the wear-corrosion process, both the solution-annealed and age-treated Fe–Mn–Al alloys had no passive region in 3% NaCl solution.

The open circuit potentials of the solution-annealed and age-treated Fe–Mn–Al alloys in 3% NaCl solution increased with increasing rotation speed during the erosion-corrosion process, but decreased with increasing rotation speed and contact load during the wear-corrosion process.

The weight loss of the solution-annealed Fe–Mn–Al alloy during 90-h wear-corrosion test in 3% NaCl solution was about two times larger than that of the age-treated Fe–Mn–Al alloy with the presence of β-Mn.

After potentiodynamic polarization curve measurements during erosion- and wear-corrosion tests, the scanning electron microscope observations showed that the ferrite phase in the solution-annealed Fe–Mn–Al alloy was prone to corrode with respect to the austenite phase. However, for the age-treated Fe–Mn–Al alloy, corrosion preferentially occurred in the austenite phase region where β-Mn precipitated.

Acknowledgements

The authors gratefully acknowledge the financial support for this research by the National Science Council of the Republic of China under contract no. NSC 80-0405-E002-06.

References

[1] S.K. Banerji, Metal Prog. 113 (1978) 59.
[2] J.S. Duming, M.L. Glenn, H.W. Leavenworth Jr, Metal Prog. 126 (1984) 19.
[3] R. Wang, M.J. Straszheim, R.A. Rapp, Oxidation Metal. 21 (1984) 71.
[4] R. Wang, R.A. Rapp, in: Proceedings of the 9th International Corrosion Congress, Toronto, Canada, Vol. 4, 1984, p. 545.

[5] R. Wang, F.H. Beck, Metal Prog. 123 (1983) 72.
[6] J.Y. Liu, S.C. Chang, J. Mater. Sci. 31 (1996) 4159.
[7] P. Tomaszewicz, G.R. Wallwork, Corrosion 40 (1984) 152.
[8] V.G. Rivlin, Int. Metal. Rev. 28 (1983) 309.
[9] W.T. Tsai, J.B. Duh, J.T. Lee, J. Mater. Sci. 22 (1987) 3517.
[10] S.C. Chang, W.H. Weng, H.C. Chen, S.J. Lin, P.C.K. Chung, Wear 181-183 (1995) 511.
[11] H.H. Huang, Master Thesis, National Central University, Chung-Li, Taiwan, Republic of China, 1989.
[12] S.C. Chang, T.S. Sheu, C.M. Wan, in: Proceedings of the 7th International Conference on the Strength and Metals and Alloys, Montreal, Canada, 12–16 August, 1985, p. 1081.
[13] G.K. Nathan, W.J.D. Jones, Wear 9 (1966) 300.